Early Aβ Reduction Prevents Progression of Cerebral Amyloid Angiopathy

Juliane Schelle, PhD,[1,2†] Bettina M. Wegenast-Braun, PhD,[1,2†] Sarah K. Fritschi, PhD,[1,2] Stephan A. Kaeser, MS,[1,2] Nina Jährling, PhD,[3,4] Daniel Eicke, MS,[1,2] Angelos Skodras, PhD,[1,2] Natalie Beschorner, MS,[1,2] Ulrike Obermueller,[1,2] Lisa M. Häsler, MS,[1,2] David P. Wolfer, MD,[5] Thomas Mueggler, PhD,[6] Derya R. Shimshek, PhD,[7] Ulf Neumann, PhD,[7] Hans-Ulrich Dodt, PhD,[3,4] Matthias Staufenbiel, PhD,[2] and Mathias Jucker, PhD [1,2]

Objective: Clinical trials targeting β-amyloid peptides (Aβ) for Alzheimer disease (AD) failed for arguable reasons that include selecting the wrong stages of AD pathophysiology or Aβ being the wrong target. Targeting Aβ to prevent cerebral amyloid angiopathy (CAA) has not been rigorously followed, although the causal role of Aβ for CAA and related hemorrhages is undisputed. CAA occurs with normal aging and to various degrees in AD, where its impact and treatment is confounded by the presence of parenchymal Aβ deposition.
Methods: APPDutch mice develop CAA in the absence of parenchymal amyloid, mimicking hereditary cerebral hemorrhage with amyloidosis Dutch type (HCHWA-D). Mice were treated with a β-site amyloid precursor protein cleaving enzyme 1 (BACE1) inhibitor. We used 3-dimensional ultramicroscopy and immunoassays for visualizing CAA and assessing Aβ in cerebrospinal fluid (CSF) and brain.
Results: CAA onset in mice was at 22 to 24 months, first in frontal leptomeningeal and superficial cortical vessels followed by vessels penetrating the cortical layers. CSF Aβ increased with aging followed by a decrease of both Aβ40 and Aβ42 upon CAA onset, supporting the idea that combined reduction of CSF Aβ40 and Aβ42 is a specific biomarker for vascular amyloid. BACE1 inhibitor treatment starting at CAA onset and continuing for 4 months revealed a 90% Aβ reduction in CSF and largely prevented CAA progression and associated pathologies.
Interpretation: This is the first study showing that Aβ reduction at early disease time points largely prevents CAA in the absence of parenchymal amyloid. Our observation provides a preclinical basis for Aβ-reducing treatments in patients at risk of CAA and in presymptomatic HCHWA-D.

ANN NEUROL 2019;86:561–571

Cerebral amyloid angiopathy (CAA) is common in the elderly and associated with cerebrovascular alterations and an increased risk of intracerebral bleeding.[1,2] CAA is thought to contribute to hemorrhagic stroke but also to compromise normal brain function, including cognition. It progressively increases with aging, both in frequency

View this article online at wileyonlinelibrary.com. DOI: 10.1002/ana.25562

Received Mar 15, 2019, and in revised form Jul 24, 2019. Accepted for publication Jul 24, 2019.

Address correspondence to Dr Jucker, Hertie-Institute for Clinical Brain Research, University of Tübingen, Otfried-Müller Strasse 27, D-72076 Tübingen, Germany.
E-mail: mathias.jucker@uni-tuebingen.de

[†]J.S. and B.M.W.-B. contributed equally.

Current address for Dr Mueggler: Roche Pharma Research & Early Development, Neuroscience, Basel, Switzerland.

From the [1]German Center for Neurodegenerative Diseases, Tübingen, Germany; [2]Department of Cellular Neurology, Hertie Institute for Clinical Brain Research, University of Tübingen, Tübingen, Germany; [3]TU Wien, Vienna, Austria; [4]Center for Brain Research, Medical University of Vienna, Vienna, Austria; [5]Institute of Anatomy, University of Zürich, Zürich, Switzerland; [6]Institute for Biomedical Engineering, University and Swiss Federal Institute for Technology, Zürich, Switzerland; and [7]Novartis Institutes for Biomedical Research, Basel, Switzerland

Additional supporting information can be found in the online version of this article.

and severity, and is also commonly observed in Alzheimer disease (AD). CAA is caused by deposition of aggregated β-amyloid peptides (Aβ) within cerebral vessels.[1] The most prominent Aβ isoform deposited is Aβ40 (the Aβ species ending at amino acid 40). This is in contrast to the parenchymal plaques in AD brain that contain primarily the Aβ42 isoform.[3] CAA can develop sporadically or can be linked to distinct mutations in the Aβ precursor protein (APP). Patients with an APP E693Q mutation develop severe CAA in the virtual absence of compact (congophilic) parenchymal plaques (hereditary cerebral hemorrhage with amyloidosis Dutch type [HCHWA-D]).[4,5]

Similar to humans, different Aβ plaque-forming APP transgenic mouse models also develop CAA to quite a different degree.[6] In an attempt to generate a "pure" CAA model, we took advantage of the HCHWA-D mutation, which resulted in an especially clean recapitulation of the CAA-only phenotype in APPDutch mice.[7] These mice develop CAA in leptomeningeal and cortical vessels together with smooth muscle and basement membrane disruptions, gliosis, and microhemorrhages. As in humans, vascular amyloid in APPDutch mice consists largely of Aβ40. Interestingly, amyloid deposition in APPDutch mice can be directed to parenchymal plaques upon additional expression of mutated presenilin 1 that shifts Aβ generation to the longer Aβ42 isoforms.[8] This observation further emphasizes the close mechanistic link between CAA and parenchymal amyloid and their corresponding clinically distinct phenotypes.[9]

Currently, no treatment for CAA is available. In fact, some Aβ immunotherapies both in AD patients and mouse models resulted in increased CAA, blood vessel–associated bleeding, or amyloid-related imaging abnormalities, even with overall reduced Aβ deposition. These observations suggest a complex, dynamic interaction between the different Aβ isoforms and assemblies as well as antibodies.[10–14] To focus on the treatment of CAA and to avoid interference by parenchymal Aβ deposition, we used the APPDutch mouse model. We further focused on very early disease stages and thus aimed at preventing CAA progression rather than clearing vascular Aβ deposition with putative side effects. To this end, we used an inhibitor of β-site APP-cleaving enzyme 1 (BACE1), which decreases Aβ production. Our results demonstrate that Aβ reduction at such early time points considerably delays the development and progression of CAA and associated pathologies.

Materials and Methods

Mice

APPDutch mice overexpress E693Q mutated human APP751 under the neuron-specific murine Thy-1 promoter element.[7] The mice have been generated and maintained on a C57BL/6J (B6) background. Animals were kept in standard housing conditions with a 12-hour dark/light cycle with free access to food and water. The mean life span of APPDutch mice is about 26 to 28 months, similar to their nontransgenic littermates and similar to B6 mice.[7,15] CAA onset in female APPDutch mice is around 22 to 24 months, and in males CAA onset is delayed.[7] Thus to increase the chance that the mice in the present study would develop robust CAA, only female mice were included in the treatment study. All experiments were in compliance with protocols approved by the local Animal Care and Use Committees (N5/13, N2/15, and N10/15). The exact number of mice used for each experiment is given in the figure legends.

BACE1 Inhibitor Treatment

The BACE1 inhibitor NB-360 (Novartis, Basel, Switzerland) was mixed into standard food pellets (0.5g NB-360/kg food pellets). This dose yields brain exposure similar to 100μmol/kg orally, as previously described.[16,17] Average plasma and brain levels of NB-360 over 24 hours for this dose were 1.2 and 4.8μM, respectively.[17] Two batches of female APPDutch mice were fed with pellets containing the BACE1 inhibitor NB-360 between ages 23.5 and 27.5 months. Age-matched female control mice received control pellets without the drug for the same time period. Food pellets were available ad libitum until the mice were killed. Animals were monitored daily by animal caretaker staff and 3 times a week by the researchers during the entire treatment period. There were no differences in food consumption and body weight between BACE1 inhibitor–treated mice and control mice.

Cerebrospinal Fluid and Brain Collection

Cerebrospinal fluid (CSF) collection has been described previously and was always done between 10 AM to 2 PM on a given day to minimize circadian CSF Aβ variations.[17–19] Deeply anesthetized mice (ketamine at 100mg/ml and xylazine at 10mg/ml) were kept on a heating pad during the whole procedure to avoid hypothermia. With the help of a dissecting microscope, the skin was opened and the underlying tissue and neck muscles were separated to expose the cisterna magna. The dura mater was perforated, and the CSF was collected with a GELoader Tip (Eppendorf, Hamburg, Germany).[17] CSF samples were immediately centrifuged at $2{,}000 \times g$ for 10 minutes (at room temperature) and inspected for blood contamination. Aliquots were stored at −80°C until use. After CSF collection, mice were perfused for 4 minutes with phosphate-buffered saline (PBS) at 4°C. The brain was removed, and one hemisphere was snap frozen on dry ice. The other hemibrain was immersion fixed in 4% paraformaldehyde (in 0.1M PBS for 48 hours at 4°C), immersed in 30% sucrose in PBS for additional 48 hours at 4°C, and then frozen in 2-methylbutane. Both hemispheres were stored at −80°C until use.

Ultramicroscopy

To visualize the 3-dimensional (3D) distribution of vascular amyloid in APPDutch mouse brain, mice (n = 4, 28–31 months of age) were injected twice (24-hour interval) intraperitoneally with 75μl of 1% methoxy-X04 (courtesy of W. Klunk, University of Pittsburgh)[20] in dimethyl sulfoxide. Two hours after the

last injection, animals were deeply anesthetized and perfused transcardially with the following ice-cold solutions: 10ml of heparin-sodium (5 IE/ml; B. Braun Melsungen AG, Melsungen, Germany) in PBS, 20ml of 1% paraformaldehyde in PBS, 20ml of 0.001% fluorescein isothiocyanate (FITC)-labeled *Lycopersicon esculentum* lectin (tomato lectin; Vector Laboratories, Burlingame, CA) in PBS, and finally 50ml of 4% paraformaldehyde in PBS. Subsequently, brains were prepared and postfixed in 4% paraformaldehyde in PBS at 4°C overnight, followed by 3 washes in PBS. The tissue was dehydrated in an ascending series of ethanol concentrations (50%, 70%, 80%, 96% for 24 hours, 4 × 100% for 24 hours) and transferred into the peroxide-free clearing medium, containing 1 part benzyl alcohol and 2 parts benzyl benzoate.[21] The brains were kept in this clearing solution until they became transparent.[22] Two-sided light sheet illumination was performed using a Sapphire diode laser with λ = 488nm (Coherent, Dieburg, Germany; 500mW) and a LQC 180E diode laser with λ = 405nm (Newport, Irvine, CA; 180mW). The LQC 180E diode laser was integrated into the setup by using a dichroic mirror.[23] Unwanted excitation light was blocked in the observation pathway by an ET 525/50 bandpass filter (AHF Analysentechnik, Tübingen, Germany) for the 488nm laser and an E 455 long pass filter (Chroma Technology, Bellows Falls, VT) for the 405nm laser. Image recording was performed using Olympus XL Fluor objectives (2×: N.A. 0.14; 4: N.A. 0.28 (N.A. stands for Numerical Aperture); Olympus, Tokyo, Japan) and a 12-bit CCD camera with 2,048 × 2,048-pixel resolution (Cool Snap K4; Roper Scientific, Planegg, Germany). For visualizing the entire brain, a 0.63× postdemagnification was combined with the 2× objective. The 3D image reconstruction was performed via Amira 5.2 (Visage Imaging, Berlin, Germany).

Aβ Measurement in CSF and Brain

Aβ40 (Aβx–40) and Aβ42 (Aβx–42) concentrations in CSF and brain extracts (frozen hemisphere, see previous description) were determined with an electrochemiluminescence-linked immunoassay (V-PLEX Aβ Peptide Panel 1 [6E10] Kit; Meso Scale Discovery, Gaithersburg, MD). CSF was diluted 1:14 in buffer (Diluent 35; Meso Scale Discovery) and analyzed according to the manufacturer's instructions, as described previously.[17] Forebrains (hemibrains without cerebellum) were homogenized at 10% (weight/volume) in homogenization buffer (50mM Tris pH 8.0, 150mM NaCl, 5mM EDTA, and protease/phosphatase inhibitor cocktail from Thermo Fisher Scientific, Waltham, MA) at 4°C using 7ml lysing tubes with 2.8mm ceramic beads and a tissue homogenizer (Precellys; Bertin Technologies, Montigny-le-Bretonneux, France) twice at 5,500 rpm for 10 seconds (with a break of 10 seconds). The homogenized brain tissue was aliquoted and stored at −80°C until use. For Aβ measurements, the homogenates were extracted as follows: aliquots were thawed on ice, mixed 1:3.2 with cold formic acid (FA) at minimum 96% purity (Millipore; Sigma, St Louis, MO), sonicated for 35 seconds at 4°C, and spun at 25,000 × *g* at 4°C for 1 hour. The supernatant was collected as the "FA-soluble fraction" and equilibrated (1:20) in neutralization buffer (1M Tris base, 0.5M Na_2HPO_4, 0.05% NaN_3). FA-soluble total brain extracts were diluted up to 1:4 in buffer (Diluent 35; Meso Scale Discovery) before measurement. Data analysis used MSD Discovery Workbench software 2.0. Internal reference samples were used as controls in every plate.

Histology and Immunohistochemistry

After freezing, fixed hemispheres were cut into serial 25µm-thick coronal sections using a freezing-sliding microtome (Leica, Nussloch, Germany). The sections were collected in tissue cryoprotection solution (35% ethylene glycol, 25% glycerol in PBS) and stained immunohistochemically according to previously published protocols using anti-Aβ polyclonal antibody CN6 (1:2,000), a follow-up version of CN3.[24] Microglia were visualized using a rabbit polyclonal antibody against ionized calcium binding adapter molecule 1 (Iba1; Thermo Fisher Scientific, catalogue no. PA5-21274) in combination with Congo red staining.[7,24] The Prussian blue reaction of Perls was used to visualize ferric iron in hemosiderin.[25,26]

For direct comparison of the 2 different Aβ staining approaches (ultramicroscopy vs Aβ immunohistochemistry), identical brain sections were first stained with methoxy-X04 (provided by W. Klunk, Pittsburgh, PA) followed by a subsequent immunohistochemical staining for Aβ (CN6). Staining with methoxy-X04 included 3 washes in PBS, a 30-minute incubation in 0.3% Triton X-100 in PBS, followed by incubation with a staining solution of 4% volume of 10mg/ml methoxy-X04 in dimethyl sulfoxide and 7.7% volume CremophorEL (Sigma-Aldrich, Steinheim, Germany) in 88.3% volume PBS for 30 minutes at room temperature, with subsequent PBS washes and final mounting with FluorSave Reagent (Merck Chemicals, Darmstadt, Germany). After images of methoxy-X04–positive vessels were acquired with a Zeiss Axioplan 2 fluorescent microscope (Carl Zeiss MicroImaging, Jena, Germany) using filter set 10 (BP 450-490 for excitation and BP 515-565 for emission; Zeiss) with a Zeiss AxioCam HR digital color camera in black-and-white mode (standard mono) and a Zeiss Plan-Neofluar 10×/0.3 objective, coverslips were removed and Aβ immunostaining was performed. Subsequently, bright-field images of Aβ immunohistochemical staining at the identical positions were acquired using no filter and the RGB mode (standard color) of the AxioCam HR camera.

For double labeling of Aβ and smooth muscle actin (SMA), sections were incubated in citrate buffer (0.04M sodium citrate dihydrate and 0.06M citric acid in distilled water, pH 6) for 30 minutes at 90°C. After a washing step with PBS, sections were treated with proteinase K (1µg/µl in 50mM Tris base and 1mM calcium chloride in distilled water, pH 7.6) for 30 minutes at 37°C. Sections were incubated for 3 days at 4°C with CN6 (anti-Aβ; 1:1,000; see previous description) and anti-alpha SMA antibody ab21027 (goat polyclonal, 1:200; Abcam, Cambridge, UK). Secondary antibodies were donkey anti-rabbit Alexa Fluor 568 (A10042, Invitrogen, Carlsbad, CA), and donkey anti-goat Alexa Fluor 488 (705-545-147; Dianova, Hamburg, Germany), both diluted 1:250. We used 4′-6-diamidino-2-phenylindole (DAPI) as a nucleic acid counterstain at 1:1,000 (D9542; Sigma, Deisenhofen, Germany). Sections were mounted with Dako

Fluorescence Mounting Medium (S3023; Biozol Diagnostica, Eching, Germany).

CAA Quantification

CAA was quantified on Aβ-immunostained (CN6 antibody) sets of every 12th systematically sampled 25μm-thick coronal section through the fixed hemisphere (see previous description). The number and severity of Aβ-positive vessels throughout the neocortex including the leptomeningeal vessels was manually assessed by a rater blinded to the experimental groups using a Zeiss Axioskop 2 microscope with a 10× objective (Zeiss, Oberkochen, Germany) as previously described in detail.[27] In short, CAA frequency refers to the number of Aβ-immunostained vessel profiles with neighboring profiles considered as separate vessels. Severity was graded in 3 categories: CAA grade 1, Aβ-immunoreactivity restricted to parts of the vessel wall; CAA grade 2, Aβ-immunoreactivity throughout the vessel wall and/or extending focally to the surrounding neuropil; CAA grade 3, extensive infiltration of Aβ into the parenchyma with a complete "amyloid coat" around the vessel.[27] If CAA frequency was zero (n = 2 animals), vessel severity was also set to zero. CAA score for an animal was calculated by multiplying CAA frequency with CAA severity.[27]

Quantification of Cerebral Hemorrhage

Perls Berlin blue–stained hemosiderin-positive microglia were quantified on an additional set of every 12th systematically sampled section throughout the neocortex and the overlying leptomeningeal vessels of the fixed hemisphere. Hemosiderin-positive staining in the vicinity of vessels and clusters of positive microglia were counted as indicators of microbleeds. Frequency of microbleeds and severity of microbleeds was assessed as previously described,[11] and the rater was blinded toward experimental groups. The microhemorrhage score was calculated by multiplying microbleed frequency with microbleed severity.[11]

Quantification of Microgliosis

Congo red–positive vessels with associated clusters of activated (hypertrophic) Iba1-positive microglia were counted in the area of the frontal cortex supplied by the medial cerebral artery (and thus robustly affected by CAA). Therefore, the 3 "frontal sections" out of the set of every 12th systematically sampled brain section were selected (bregma anterior-posterior 0.7–1.7mm) and scanned using an automated Zeiss Axioscan.Z1 slide scanner. Images were captured at ×10 magnification. For each field of view, z stacks were acquired, and extended depth of focus images were automatically stitched to produce a full image, which was imported into Fiji (https://imagej.net/Fiji).[28] An ImageJ script was written to automate the microglia color-coding process, as follows: the red channel of the RGB image was used to exclude any Congo red staining from the classification. A preselected threshold was then used to identify microglial cells. Using the built-in "Analyze Particles" function, microglia structures were marked as regions of interest (ROI); the areas of each of the ROIs were colorized on arbitrary ranges (red: area < 50μm^2; yellow: 50μm^2 ≤ area < 80μm^2; green: 80μm^2 ≤ area < 120μm^2; blue: area ≥ 120μm^2). The resulting colorized ROIs were overlaid with the original RGB image. Thus, clusters of activated microglia around CAA became easily recognizable and were counted manually by a rater blinded toward experimental groups.

Quantification of Smooth Muscle Cells

SMA and Aβ double-labeled sections (see previous description) were analyzed with a Zeiss LSM 510 META confocal microscope (40× oil-immersion Plan Neofluar objective, 1.3 NA; Axiovert 200M). Laser lines 488nm and 543nm were used to excite Alexa Fluor 488 and Alexa Fluor 568, respectively, and 405nm for DAPI counterstain. Imaging parameters were slightly adjusted for individual vessels/images to prevent overexposure. Care was given to always acquire the maximum area covered by SMA. Images of 18 to 20 vessels of the different CAA severity grades (note that CAA grade 3 of NB-360–treated mice was rare and only 5 vessels could be sampled) and also of unaffected vessels were acquired in a subset of animals from the NB-360–treated and age-matched control mice (n = 5 per group). Only penetrating vessels of similar/comparable cutting plane and diameter were selected. Images were analyzed in a semiautomated way using a customized ImageJ script in Fiji to quantify the areas of CAA and SMA in the sampled blood vessels. Residual noise was automatically removed by basic despeckle filtering, and then the blood vessel area was manually outlined and a preselected fixed threshold was set for each channel. The area of pixels above this threshold was measured within the selected ROI. The measured SMA area was normalized to the total SMA + CAA area for further analysis.

Statistical Analysis

Prism (v6.0; GraphPad Software, San Diego, CA) was used for statistical analyses and graphics. Normal distribution was assessed using the Shapiro–Wilk test. If individual CSF and brain Aβ values were below the assay detection limit, a fixed value (detection limit of the plate where the sample was measured/√2) was imputed. Imputed values were not considered for statistical analysis of the Aβ42/40 ratio measurements. In all cases, statistical significance was set at $p < 0.05$.

Results

Distribution and Progression of CAA in Aging APPDutch Mice

In a previous study, CAA was first detected in APPDutch mice at 22 to 24 months of age.[7] To better appreciate its distribution and progression in the entire mouse brain, we examined CAA in sets of systematically sampled Aβ-immunostained sections of aged APPDutch mice (n = 20; age = 23–28.5 months). Additional mice of advanced age (n = 4; age = 28–31 months) were subjected to ultramicroscopy[29] using FITC-conjugated tomato lectin in combination with the amyloid dye methoxy-04 to visualize the entire vasculature in 3D (Fig 1, Supplementary Video; see Materials and Methods section for details). Consistent with our previous study, histological analysis revealed considerable variability in the onset and amount of CAA in these mice.[7] However, in all cases, CAA first

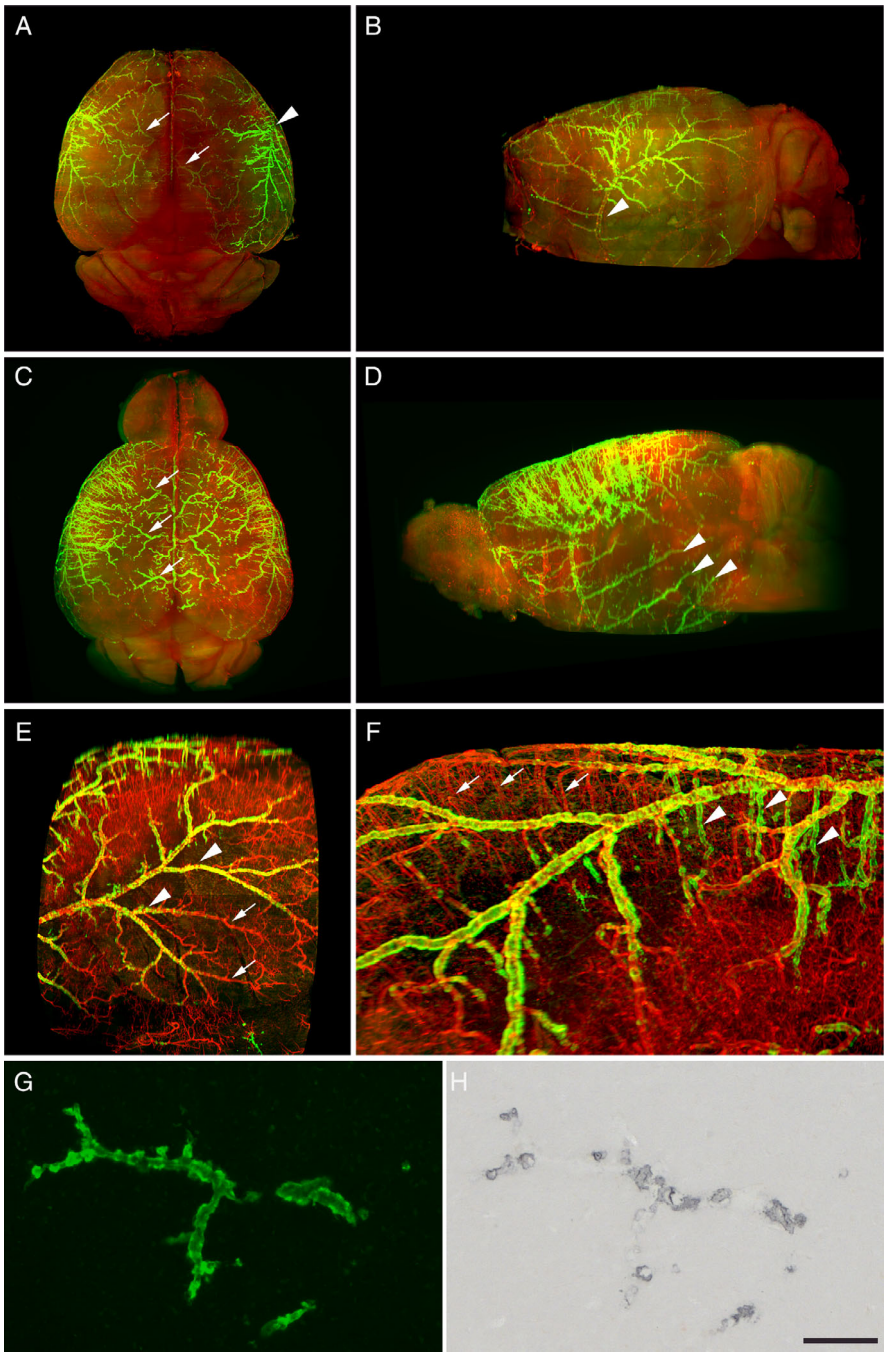

FIGURE 1: Three-dimensional (3D) visualization of cerebral amyloid angiopathy (CAA) distribution and progression in APPDutch mice with ultramicroscopy. Two aged APPDutch mice at different stages of CAA deposition are shown. (A, B) CAA deposition was first observed in the middle cerebral artery and its superficial leptomeningeal branches (*arrowheads*; moderately affected female APPDutch mouse; 30 months old; B is the lateral view of A). Minor CAA deposition was observed in the branches originating from the anterior cerebral artery *(arrows)*. Note that posterior regions of the neocortex and the cerebellum were largely spared. (C, D) At later stages, CAA progressed along branches of the middle cerebral artery (eg, ventral branches, *arrowheads*) and was also observed in the superficial branches of the middle and posterior internal frontal arteries (arising from the anterior cerebral artery; *arrows*). At these later stages, CAA deposition extended towards smaller site branches and descending parenchymal arteries. The posterior cortical regions and the cerebellum remained largely spared (shown is a more severely affected male APPDutch mouse; 31 months old; D is the lateral view of C). (E) High magnification of the middle cerebral artery (from panel B). Although the main branches *(arrowheads)* were affected with CAA, smaller site branches *(arrows)* were relatively spared. (F) High magnification and rotated view of panel E; for 3D visualization, see the Supplementary Video. Severe CAA deposition was observed in the superficial branches, but at this moderate stage of disease only few descending parenchymal vessels were positive for CAA *(arrowheads)*. Examples of unaffected penetrating arteries are marked with arrows (green: CAA stained with methoxy-X04; red: vessel counterstaining with fluorescein isothiocyanate–conjugated tomato lectin; all images are projections of 3D views with the following relative zoom factors: 0.4 (A, C; dorsal views), 0.5 (B, D; lateral views), 1.0 (E), and 1.6 (F). Overlap of a histological methoxy-X04 CAA staining (G) with a subsequent immunohistochemical staining for β-amyloid peptides of the identical section (H). This affected vessel within a 25μm brain section is from a female 28-month-old APPDutch mouse; see Materials and Methods section for details. Scale bar is 100μm.

appeared in superficial vessels of the cortex followed by vessels penetrating the cortical layers. Parenchymal deposition was very rare and if found it was of diffuse nature. Occasionally, CAA was also seen in the thalamus, the hippocampal formation, and the amygdala.

Ultramicroscopy revealed CAA first within the middle cerebral artery and its branches, with minor deposition in the branches originating from the anterior cerebral artery. The posterior regions of the neocortex and the cerebellum remained mostly unaffected (see Fig 1A–D; Supplementary Video). Within the affected arteries, most CAA was detected in the main superficial branches, and smaller side branches were spared (shown for the middle cerebral artery, see Fig 1E, F). In more heavily affected animals, branches also showed prominent CAA, and Aβ deposition was observed in descending cerebral arteries with an increased overall vessel surface occupied with amyloid. As expected, high overlap between the methoxy-X04 staining used for ultramicroscopy and Aβ-positive immunostaining was found. High magnification of methoxy-X04 stained vessels depicted the characteristic clustered staining pattern of CAA in between vascular smooth muscle cells.

Age-Related Increase in Brain Aβ

For biochemical analyses, 4 new groups of female APPDutch mice (3, 12, 23.5, and 27.5 months of age) were examined (Fig 2). Results revealed that FA-soluble Aβx–40 and Aβx–42 in brain (ie, Aβ species ending with amino acid 40 and 42) remained unchanged and at low level until the age of 23.5 months (Fig 3A, B). At that time, some animals revealed a notable increase. This is consistent with our current and previous histological analysis[7] reporting CAA onset between age 22 to 24 months. CSF Aβ increased until 23.5 months (the time of CAA onset) with a decrease thereafter (see Fig 3D, E). The Aβ42/40 ratio remained unchanged during aging in both brain and CSF (see Fig 3C, F).

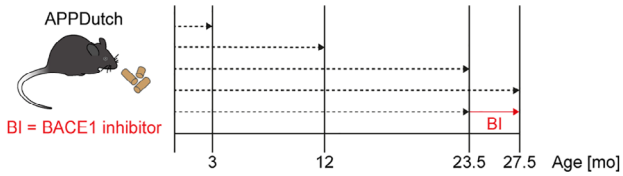

FIGURE 2: Schematic overview of aging cohorts and experimental groups. Female APPDutch mice were aged and analyzed at 3, 12, 23.5, and 27.5 months of age. An additional group of female 23.5-month-old APPDutch mice was fed with food pellets containing the β-site amyloid precursor protein cleaving enzyme 1 (BACE1) inhibitor NB-360 (BI) from age 23.5 to 27.5 months (n = 8, 9, 11, 17, and 19 for the 3, 12, 23.5, 27.5, and BI 27.5 month-old group; the higher number of mice in the 27.5-month-old groups was chosen by anticipating a higher variability). The group numbers are also mentioned again in the legends of all figures. Mice that died before the end of the experiment (n = 5 for the untreated mice and n = 6 for the BI treated mice) were not included in the analysis. Note that the mean life span of the mice is between 26 and 28 months, and thus the death of some animals was expected.

BACE Inhibition Prevented CAA Progression

APPDutch mice were treated with BACE1 inhibitor NB-360[16] starting at 23.5 months of age for 4 months (see Fig 2). NB-360 strongly reduced Aβ generation, which was revealed by a decrease of both CSF Aβ40 and Aβ42 by more than 90% compared to controls (see Fig 3D, E). This inhibition translated into a > 65% reduction of insoluble (ie, FA soluble) Aβ40 and Aβ42 (see Fig 3A, B).

Histological analysis indicated only minor CAA deposition at the 23.5-month time point, and CAA was mainly present in superficial cerebral arteries (see Fig 4A). Thereafter in untreated control mice, CAA considerably increased both in frequency and severity consistent with the histological time course and the ultramicroscopy data described. In NB-360–treated mice and in agreement with the biochemical analysis (see Fig 3), histological staining showed a strong reduction of the frequency and the severity of CAA compared to non-treated controls (see Fig 4B–D). Of note, NB-360-treated mice had less CAA in cortical parenchymal vessels, and in particular in branches originating from the anterior cerebral as well as middle cerebral artery consistent with a delay of CAA progression in BACE1 inhibitor treated mice.

CAA-Associated Pathologies

Clustering of activated microglia around vessels with moderate to severe CAA was observed in all affected animals (see Fig 5A, B), an observation in line with our previous analysis.[7] Consistent with the greatly reduced CAA in NB-360–treated mice, there was a significant reduction of CAA-associated microgliosis in the 27.5-month-old NB-360–treated mice compared to the age-matched control mice (see Fig 5C).

Microhemorrhages were rare and associated only with a small subset of amyloid-laden vessels. Large intracerebral bleeding was not observed. No difference in microhemorrhages between the 27.5-month-old NB-360–treated mice versus the nontreated control mice was found (see Fig 5D).

Progressive Aβ deposition in the vasculature (increasing CAA severity grade) led to a loss of smooth muscle cells in both the NB-360–treated 27.5-month-old mice and the control mice (see Fig 5E, F). However, since all CAA severity grades were drastically reduced in the NB-360–treated mice compared to the age-matched control

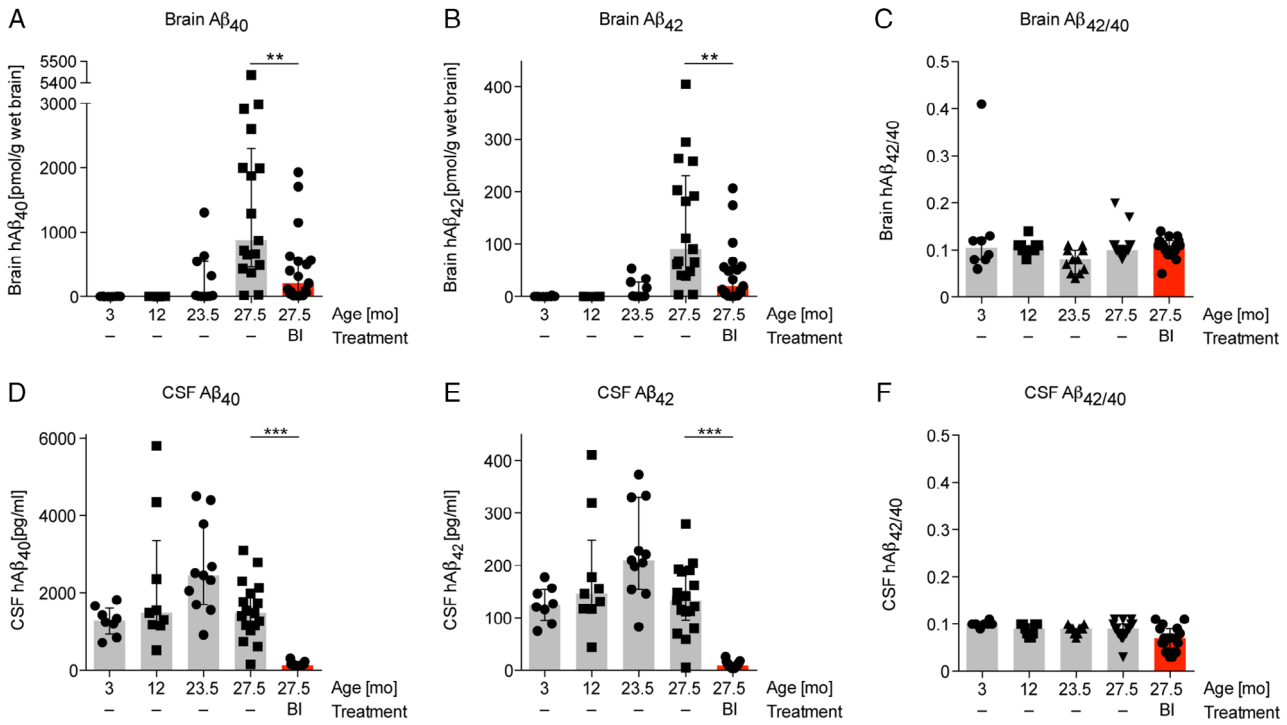

FIGURE 3: Levels of brain and cerebrospinal fluid (CSF) aggregated β-amyloid peptides (Aβ) in aging APPDutch mice and after treatment with a β-site amyloid precursor protein cleaving enzyme 1 (BACE1) inhibitor. Female APPDutch mice were aged, and half the mice (see schema in Fig 2) were fed with either control food pellets or pellets containing a BACE1 inhibitor NB-360 (BI) starting at age 23.5 months until 27.5 months. (A–C) Aβx–40 and Aβx–42 levels in brain were largely reduced by BI treatment (Mann–Whitney *U* test comparing 27.5-month-old groups: $U = 67.0$ [$p = 0.0022$] and $U = 73.0$ [$p = 0.0043$], respectively). No difference in brain Aβ42/40 ratio after BI treatment was found (C). (D–F) CSF Aβ increased from 3 to 23.5 months of age and decreased thereafter; Kruskal–Wallis H test for the 4 age groups, $df = 3$, CSF Aβx–40: H corrected for ties = 9.32 ($p = 0.025$); post hoc Dunn multiple comparisons test was employed for group comparisons, which were always conducted between the 3-month group with all other age groups: 3 versus 23.5 months, $p = 0.017$, all others $p > 0.05$ (D); CSF Aβx–42: H corrected for ties = 10.19 ($p = 0.017$), 3 versus 23.5 months, $p = 0.021$, all others $p > 0.05$ (E). Treatment with NB-360 (BI) significantly decreased CSF Aβx–40 and Aβx–42 levels compared to age-matched 27.5-month-old controls (Mann–Whitney *U* test comparing 27.5-month-old groups, $U = 5.5$ and $U = 14.0$, respectively; $p < 0.0001$). The difference in CSF Aβ42/40 ratio after BI treatment was not assessed due to the majority of imputed values within the BI group (F). All data are represented as median with interquartile range; n = 8, 9, 11, 17, and 19 for the 3, 12, 23.5, 27.5 and 27.5 BI group (see also Fig 2). *$p < 0.05$, **$p < 0.01$, ***$p < 0.001$.

mice, results reveal that BACE1 inhibition also prevented vessel-associated smooth muscle cell loss (see Fig 5G-I).

Discussion

Vascular deposition of Aβ detectable as congophilic CAA occurs with normal aging and to varying degrees also in AD, where its impact and treatment is confounded by the presence of parenchymal Aβ deposition. CAA is associated with disruption of vascular structure and hemorrhages and compromises brain function in sporadic and hereditary (eg, HCHWA-D) forms.[30] Here, we have studied the effect of Aβ reduction at the time of CAA onset in an animal model (APPDutch mice) that develops CAA in the absence of parenchymal amyloid deposition.[7]

To this end, we have expanded previous work of CAA development in the APPDutch mouse model[7] and have complemented Aβ-immunostaining on serial histological sections with 3D ultramicroscopy, which enabled visualization of the entire cortical vasculature with CAA. CAA-positive leptomeningeal vessels and vessels penetrating the cerebral cortex were mainly observed in frontal (and parietal) regions with posterior regions much less affected. CAA was also found occasionally in the thalamus, hippocampal formation, and amygdala. Except for the predilection for the frontal relative to the posterior cortices, CAA distribution in the mice resembled the observations in HCHWA-D patients, where CAA consistently is observed in meninges and cerebral cortex and only to a lesser degree in basal ganglia, hippocampus, and brainstem.[31] In APPDutch mice, vessels were sequentially affected starting at the main cerebral arteries and progressing towards smaller branches and descending parenchymal arteries. First deposition of CAA was found in the middle cerebral artery and its branches, and the anterior cerebral artery was only later affected. Over time, the area covered with amyloid increased within all affected vessels. A similar development of CAA, with an anterior-to-posterior and large-to-small vessel gradient of involvement has been described in other transgenic mouse models despite the

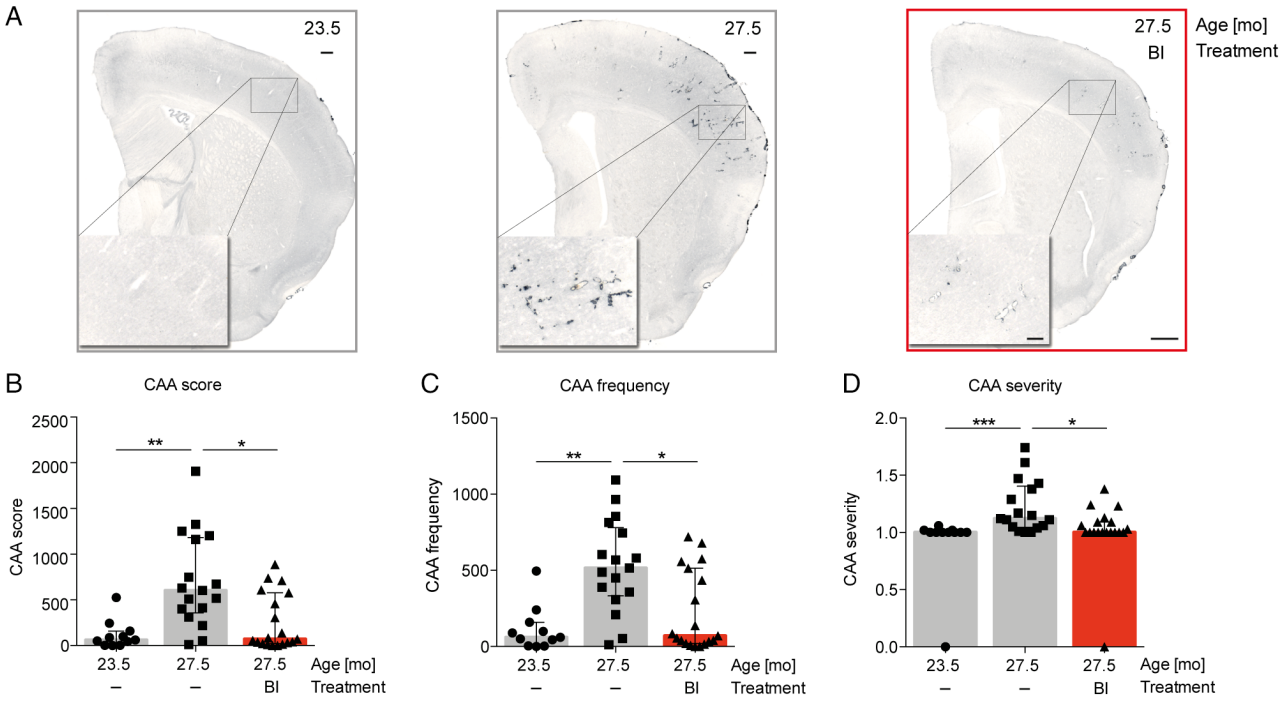

FIGURE 4: β-site amyloid precursor protein cleaving enzyme 1 (BACE1) inhibition prevents age-dependent cerebral amyloid angiopathy (CAA) progression. Female APPDutch mice (see treatment schema, Fig 2) were fed with either food pellets containing the BACE1 inhibitor NB-360 (BI) or control pellets from age 23.5 to 27.5 months. (A) CAA deposition (immunostaining for aggregated β-amyloid peptides) on coronal hemibrain sections is exemplarily shown for each group. An increase in CAA from 23.5 to 27.5 months was observed, which was in line with the histological time course and the ultramicroscopy in aging APPDutch mice. In contrast to control-treated mice, BI-treated mice showed an overall reduction in the amount of CAA, especially in branches originating from the anterior cerebral artery as well as the middle cerebral artery. Inserts depict CAA deposition in the region perfused by the middle cerebral artery and its branches (see also Fig 1; scale bars are 500μm and 100μm; please note that animals with a high CAA load are depicted to demonstrate CAA distribution). (B–D) CAA quantification of neocortex, including the leptomeningeal vessels, revealed a significant age-dependent increase between 23.5 and 27.5 months, which could be largely prevented by the application of the BACE1 inhibitor. The results are presented as CAA score (B; Kruskal–Wallis H test, *df* = 2, H corrected for ties = 13.33, *p* = 0.0013; Dunn multiple comparisons test **p* < 0.05, ***p* < 0.01), which was calculated by multiplying CAA frequency (C; Kruskal–Wallis H test, *df* = 2, H corrected for ties = 13.33, *p* = 0.0013; Dunn multiple comparisons test **p* < 0.05, ***p* < 0.01) with CAA severity (D; Kruskal–Wallis H test, *df* = 2, H corrected for ties = 15.37, *p* = 0.0005; Dunn multiple comparisons test **p* < 0.05, ****p* < 0.001). All data are represented as group medians with interquartile range; n = 11, 17, and 19 for the 23.5, 27.5, and 27.5 BI groups, respectively.

additional Aβ deposition in the brain parenchyma in these mice.[6,32]

In CSF of APPDutch mice, we observed an age-related increase of Aβ until first Aβ deposition with a decrease of Aβ thereafter. This is reminiscent to the biphasic CSF Aβ levels in other APP transgenic mice, that is, an increase in early phases and a decrease upon onset of amyloid deposition.[19] Interestingly, the decrease in CSF Aβ upon deposition was equal for Aβ40 and Aβ42 in the APPDutch model, and it appears much stronger for Aβ42 compared to Aβ40 in the APP transgenic mouse models with primarily parenchymal amyloid deposition.[19] A similar observation has been made in patients diagnosed with CAA[33,34] and was recently extended to presymptomatic HCHWA-D mutation carriers.[35] Our observations suggest that even in mice, a comparable reduction of both CSF Aβ40 and 42 is a suited and specific biomarker for vascular amyloid deposition.

Treatment of aged APPDutch mice 23.5 to 27.5 months with NB-360 led to a more than 90% reduction of CSF Aβ and demonstrates that BACE1 inhibition is also very effective in aged mice. Consistently, NB-360 remarkably prevented the increase in insoluble Aβ and the progression of CAA. Indeed, vascular amyloid was rarely seen (or at least greatly reduced) in the cortical parenchyma–penetrating branches of the anterior and middle cerebral arteries in NB-360–treated APPDutch mice. No shift of Aβ to other forms of deposits such as diffuse plaques was observed. CAA-associated microgliosis and smooth muscle cell loss were reduced in the treated mice, indicating a beneficial effect of the treatment. The number of microhemorrhages was unchanged between treated and control groups, and the lack of a reduction may be explained by the paucity of robust CAA-associated bleedings at this early stage of CAA.

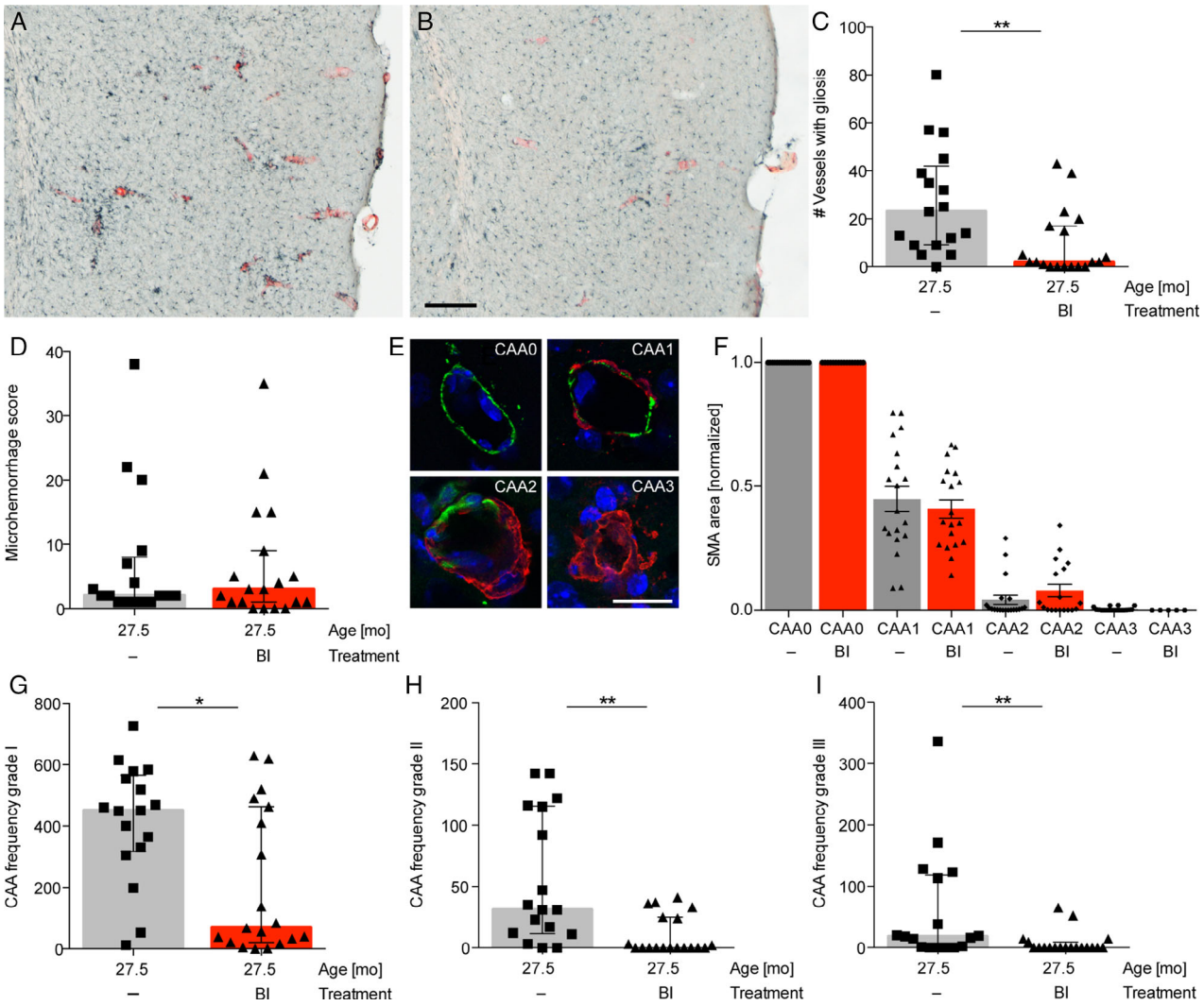

FIGURE 5: Microgliosis, microhemorrhages, and vascular smooth muscle cell loss in β-site amyloid precursor protein cleaving enzyme 1 (BACE1)-inhibitor–treated mice. Female APPDutch mice were either fed with food pellets containing the BACE1 inhibitor NB-360 (BI; n = 19) or control pellets (n = 17) for 4 months (same mice as in Figs 3, 4). (A, B) Cerebral amyloid angiopathy (CAA)–positive vessels (Congo red [CR], red) revealed clustering of activated (hypertrophic) microglia (immunostaining for ionized calcium binding adapter molecule 1, blue-black). Compared to the control mice (A), microglia clustering was reduced in the BI treatment group (B) consistent with the reduced CAA in the BI-treated mice. Images depict part of the brain region perfused by the middle cerebral artery and its branches (see also Fig 1). Scale bar is 200μm. (C) Quantification (see Materials and Methods section for details) revealed a reduction of CR-positive vessels with clusters of hypertrophic microglia in BI-treated mice compared to the controls (Mann–Whitney *U* test: $U = 69.0$, $p = 0.0026$; median with interquartile range). (D) Microhemorrhages were assessed by counting and grading clusters of hemosiderin-positive microglia in the neocortex including the leptomeningeal vessels (see Materials and Methods section for details). No significant difference between control and BI-treated mice for the calculated microhemorrhage score was found (Mann–Whitney *U* test: $U = 146.5$, $p = 0.64$; median with interquartile range). (E) Progressive loss of smooth muscle cells with increasing CAA. Double-stained vessels (smooth muscle actin [SMA], green; aggregated β-amyloid peptides, red) of different CAA severity grades (grade 1–3; see Materials and Methods section for details). Unaffected vessels (CAA0) depict a complete layer of smooth muscle cells, and CAA grade 1 (CAA1) leads to a focal displacement of smooth muscle cells. In CAA stage 3 (CAA3), there is a complete loss of the smooth muscle cells. Scale bar is 20μm. (F) Quantification of the smooth muscle cells for vessels with different CAA grades (SMA area was normalized to the total SMA + CAA area per vessel; see Materials and Methods section for details). A drastic decrease of smooth muscle cell staining with increasing CAA grade was found, and this was equally true for both groups, that is, BI treatment and controls (2-way analysis of variance, CAA severity: $df = 3$, $F = 513.45$, $p < 0.0001$; treatment: $df = 1$, $F = 0.006$, $p = 0.94$; mean and standard error of the mean is indicated). This latter observation with the finding that (G–I) frequency of all CAA severity grades was significantly reduced in the BI treated mice compared to the control mice (n = 19 and 17, respectively; Mann–Whitney *U* test, CAA1: $U = 89.0$, $p = 0.02$; CAA2: $U = 68.5$, $p = 0.002$; CAA3: $U = 71.0$, $p = 0.0017$; median with interquartile range) reveals that CAA-associated smooth muscle cell loss was largely prevented by the BI treatment.

NB-360 has not been tested in humans; however, exposures to NB-360 are very comparable to the BACE inhibitor CNP520.[36,37] CNP520 treatment of humans (90mg/day, repeated dosing) resulted in ~1μM blood levels, a blood concentration that is close to the concentration of NB-360 in mice with the current dosing

scheme.[36] Thus, the current dosing in mice appears well in the exposure range that shows CSF Aβ reduction in humans.

In conclusion, the robust prevention of CAA progression described here strongly supports testing Aβ-lowering treatments in presymptomatic HCHWA-D mutation carriers. BACE1 inhibitors appear to be a reasonable choice provided the present findings (in females) can be generalized to male mice and that recent controversies about their safety profiles for long-term treatment[38] can be resolved. For clinical trials, recent promising imaging modalities such as positron emission tomography for CAA,[39–41] functional magnetic resonance imaging (MRI) for vascular dysfunction,[42] and MRI for detection of cerebral (micro) bleeds and early blood-brain barrier breakdown[43,44] in HCHWA-D will be important requirements because CSF Aβ—albeit a good readout for vascular amyloid deposition and for target engagement—will be less optimal for assessing CAA upon BACE1 inhibitor treatment or any other Aβ-lowering therapies. Aβ-targeting clinical trials have so far largely failed for a variety of reasons, one of which is the uncertainty of Aβ's precise role in AD pathogenesis.[45,46] The link between Aβ deposition in the vasculature and CAA and associated lesions is more direct, thus increasing the chance of success in Aβ-lowering trials in patients at risk of CAA.

Acknowledgment

We thank S. Grathwohl for the experimental help and W. Klunk (University of Pittsburgh) for methoxy-X04. This work was supported by the Federal Ministry of Education and Research, Germany (BMBF ARREST-AD) and by the Austrian Theodor Körner Fund.

Author Contributions

J.S., B.M.W.-B, M.S., and M.J. contributed to the conception and design of the study; J.S., B.M.W.-B, S.K.F., S.A.K., N.J., D.E., A.S., N.B., U.O., L.M.H., D.P.W., T.M., D.R.S., U.N., and H.-U.D. contributed to the acquisition and analysis of data; J.S., B.W.M.B., S.K.F., D.E., M.S., and M.J. with the help of the coauthors contributed to drafting the text and preparing the figures.

Potential Conflicts of Interest

U.N. and D.S. are employees and shareholders of Novartis Pharma AG, Basel, Switzerland. All other authors have nothing to report.

References

1. Charidimou A, Boulouis G, Gurol ME, et al. Emerging concepts in sporadic cerebral amyloid angiopathy. Brain 2017;140:1829–1850.
2. Yamada M. Cerebral amyloid angiopathy: emerging concepts. J Stroke 2015;17:17–30.
3. Herzig MC, Van Nostrand WE, Jucker M. Mechanism of cerebral beta-amyloid angiopathy: murine and cellular models. Brain Pathol 2006;16:40–54.
4. Maat-Schieman ML, Yamaguchi H, van Duinen SG, et al. Age-related plaque morphology and C-terminal heterogeneity of amyloid beta in Dutch-type hereditary cerebral hemorrhage with amyloidosis. Acta Neuropathol 2000;99:409–419.
5. Kamp JA, Moursel LG, Haan J, et al. Amyloid β in hereditary cerebral hemorrhage with amyloidosis-Dutch type. Rev Neurosci 2014;25: 641–651.
6. Jakel L, Van Nostrand WE, Nicoll JAR, et al. Animal models of cerebral amyloid angiopathy. Clin Sci (Lond) 2017;131:2469–2488.
7. Herzig MC, Winkler DT, Burgermeister P, et al. Abeta is targeted to the vasculature in a mouse model of hereditary cerebral hemorrhage with amyloidosis. Nat Neurosci 2004;7:954–960.
8. Herzig MC, Paganetti P, Staufenbiel M, Jucker M. BACE1 and mutated presenilin-1 differently modulate Abeta40 and Abeta42 levels and cerebral amyloidosis in APPDutch transgenic mice. Neurodegener Dis 2007;4:127–135.
9. Thomason LA, Stefanovic B, McLaurin J. Cerebrovascular contributions to Alzheimer's disease pathophysiology and potential therapeutic interventions in mouse models. Eur J Neurosci 2013;37: 1994–2004.
10. Boche D, Zotova E, Weller RO, et al. Consequence of Abeta immunization on the vasculature of human Alzheimer's disease brain. Brain 2008;131:3299–3310.
11. Pfeifer M, Boncristiano S, Bondolfi L, et al. Cerebral hemorrhage after passive anti-Abeta immunotherapy. Science 2002;298:1379.
12. Salloway SP, Sperling R, Fox NC, et al. Long-term follow up of patients with mild-to-moderate Alzheimer's disease treated with bapineuzumab in a phase III, open-label, extension study. J Alzheimers Dis 2018;64:689–707.
13. Sperling RA, Jack CR Jr, Black SE, et al. Amyloid-related imaging abnormalities in amyloid-modifying therapeutic trials: recommendations from the Alzheimer's Association Research Roundtable Workgroup. Alzheimers Dement 2011;7:367–385.
14. Bales KR, O'Neill SM, Pozdnyakov N, et al. Passive immunotherapy targeting amyloid-β reduces cerebral amyloid angiopathy and improves vascular reactivity. Brain 2016;139:563–577.
15. Jucker M, Ingram DK. Murine models of brain aging and age-related neurodegenerative diseases. Behav Brain Res 1997;85:1–26.
16. Neumann U, Rueeger H, Machauer R, et al. A novel BACE inhibitor NB-360 shows a superior pharmacological profile and robust reduction of amyloid-β and neuroinflammation in APP transgenic mice. Mol Neurodegener 2015;10:44.
17. Schelle J, Hasler LM, Gopfert JC, et al. Prevention of tau increase in cerebrospinal fluid of APP transgenic mice suggests downstream effect of BACE1 inhibition. Alzheimers Dement 2017;13:701–709.
18. Maia LF, Kaeser SA, Reichwald J, et al. Changes in amyloid-β and Tau in the cerebrospinal fluid of transgenic mice overexpressing amyloid precursor protein. Sci Transl Med 2013;5:194re2.
19. Maia LF, Kaeser SA, Reichwald J, et al. Increased CSF Aβ during the very early phase of cerebral Aβ deposition in mouse models. EMBO Mol Med 2015;7:895–903.
20. Klunk WE, Bacskai BJ, Mathis CA, et al. Imaging Abeta plaques in living transgenic mice with multiphoton microscopy and methoxy-X04, a systemically administered Congo red derivative. J Neuropathol Exp Neurol 2002;61:797–805.

21. Klymkowsky MW, Hanken J. Whole-mount staining of Xenopus and other vertebrates. Methods Cell Biol 1991;36:419–441.

22. Jahrling N, Becker K, Saghafi S, Dodt HU. Light-sheet fluorescence microscopy: chemical clearing and labeling protocols for ultramicroscopy. Methods Mol Biol 2017;1563:33–49.

23. Becker K, Jahrling N, Kramer ER, et al. Ultramicroscopy: 3D reconstruction of large microscopical specimens. J Biophotonics 2008;1:36–42.

24. Eisele YS, Obermuller U, Heilbronner G, et al. Peripherally applied Abeta-containing inoculates induce cerebral beta-amyloidosis. Science 2010;330:980–982.

25. Carson FL. *Histotechnology*. 2nd ed. Chicago, IL: American Society for Clinical Pathology, 1996.

26. Gomori G. Microtechnical demonstration of iron: a criticism of its methods. Am J Pathol 1936;12:655–664.

27. Winkler DT, Bondolfi L, Herzig MC, et al. Spontaneous hemorrhagic stroke in a mouse model of cerebral amyloid angiopathy. J Neurosci 2001;21:1619–1627.

28. Schindelin J, Arganda-Carreras I, Frise E, et al. Fiji: an open-source platform for biological-image analysis. Nat Methods 2012;9:676–682.

29. Dodt HU, Leischner U, Schierloh A, et al. Ultramicroscopy: three-dimensional visualization of neuronal networks in the whole mouse brain. Nat Methods 2007;4:331–336.

30. Wermer MJH, Greenberg SM. The growing clinical spectrum of cerebral amyloid angiopathy. Curr Opin Neurol 2018;31:28–35.

31. Maat-Schieman M, Roos R, van Duinen S. Hereditary cerebral hemorrhage with amyloidosis-Dutch type. Neuropathology 2005;25:288–297.

32. Domnitz SB, Robbins EM, Hoang AW, et al. Progression of cerebral amyloid angiopathy in transgenic mouse models of Alzheimer disease. J Neuropathol Exp Neurol 2005;64:588–594.

33. Renard D, Castelnovo G, Wacongne A, et al. Interest of CSF biomarker analysis in possible cerebral amyloid angiopathy cases defined by the modified Boston criteria. J Neurol 2012;259:2429–2433.

34. Verbeek MM, Kremer BP, Rikkert MO, et al. Cerebrospinal fluid amyloid beta(40) is decreased in cerebral amyloid angiopathy. Ann Neurol 2009;66:245–249.

35. van Etten ES, Verbeek MM, van der Grond J, et al. β-amyloid in CSF: biomarker for preclinical cerebral amyloid angiopathy. Neurology 2017;88:169–176.

36. Neumann U, Machauer R, Shimshek DR. The β-secretase (BACE) inhibitor NB-360 in preclinical models: from amyloid-β reduction to downstream disease-relevant effects. Br J Pharmacol https://doi.org/10.1111/bph.14582. [Epub ahead of print].

37. Neumann U, Ufer M, Jacobson LH, et al. The BACE-1 inhibitor CNP520 for prevention trials in Alzheimer's disease. EMBO Mol Med 2018;10. pii: e9316.

38. Egan MF, Kost J, Tariot PN, et al. Randomized trial of verubecestat for mild-to-moderate Alzheimer's disease. N Engl J Med 2018;378:1691–1703.

39. Baron JC, Farid K, Dolan E, et al. Diagnostic utility of amyloid PET in cerebral amyloid angiopathy-related symptomatic intracerebral hemorrhage. J Cereb Blood Flow Metab 2014;34:753–758.

40. Johnson KA, Gregas M, Becker JA, et al. Imaging of amyloid burden and distribution in cerebral amyloid angiopathy. Ann Neurol 2007;62:229–234.

41. Ly JV, Donnan GA, Villemagne VL, et al. C-11-PIB binding is increased in patients with cerebral amyloid angiopathy-related hemorrhage. Neurology 2010;74:487–493.

42. van Opstal AM, van Rooden S, van Harten T, et al. Cerebrovascular function in presymptomatic and symptomatic individuals with hereditary cerebral amyloid angiopathy: a case-control study. Lancet Neurol 2017;16:115–122.

43. Nation DA, Sweeney MD, Montagne A, et al. Blood-brain barrier breakdown is an early biomarker of human cognitive dysfunction. Nat Med 2019;25:270–276.

44. Tsai HH, Tsai LK, Chen YF, et al. Correlation of cerebral microbleed distribution to amyloid burden in patients with primary intracerebral hemorrhage. Sci Rep 2017;7:44715.

45. Castellani RJ, Plascencia-Villa G, Perry G. The amyloid cascade and Alzheimer's disease therapeutics: theory versus observation. Lab Invest 2019;99:958–970.

46. Golde TE, DeKosky ST, Galasko D. Alzheimer's disease: the right drug, the right time. Science 2018;362:1250–1251.